Monthly Notices
of the
ROYAL ASTRONOMICAL SOCIETY

Mon. Not. R. Astron. Soc. **400,** 1241–1246 (2009) doi:10.1111/j.1365-2966.2009.15550.x

Observations of 'wisps' in magnetohydrodynamic simulations of the Crab Nebula

N. F. Camus,[1⋆] S. S. Komissarov,[1⋆] N. Bucciantini[2] and P. A. Hughes[3]

[1]*Department of Applied Mathematics, The University of Leeds, Leeds LS2 9JT*
[2]*Astronomy Department, University of California at Berkeley, 601 Campbell Hall, Berkeley, CA 94720, USA*
[3]*Astronomy Department, University of Michigan, Ann Arbor, MI 48109-1042, USA*

Accepted 2009 August 14. Received 2009 August 14; in original form 2009 July 21

ABSTRACT

In this paper, we describe results of new high-resolution axisymmetric relativistic magnetohydrodynamic (MHD) simulations of pulsar wind nebulae. The simulations reveal strong breakdown of the equatorial symmetry and highly variable structure of the pulsar wind-termination shock. The synthetic synchrotron maps, constructed using a new more accurate approach, show striking similarity with the well-known images of the Crab Nebula obtained by *Chandra* and the *Hubble Space Telescope*. In addition to the jet–torus structure, these maps reproduce the Crab's famous moving wisps whose speed and rate of production agree with the observations. The variability is then analysed using various statistical methods, including the method of structure function and wavelet transform. The results point towards the quasi-periodic behaviour with the periods of 1.5–3 years and MHD turbulence on scales below 1 year. The full account of this study will be presented in a follow-up paper.

Key words: MHD – radiation mechanisms: non-thermal – relativity – methods: numerical – pulsars: individual: Crab – supernova remnants.

1 INTRODUCTION

The Crab Nebula is the archetypal compact synchrotron nebula, continuously powered by a magnetized, ultrarelativistic wind from a young, rapidly rotating neutron star. In order to match the subrelativistic expansion of the confining medium [either interstellar medium (ISM) or supernova remnant (SNR)], the wind must be decelerated. This occurs at a strong termination shock, established at a radius where the ram pressure of the pulsar wind (PW) matches the pressure of its surrounding (Rees & Gunn 1974; Kennel & Coroniti 1984a). This shock causes heating of the wind plasma and presumably particle acceleration. As a result, a bubble of relativistic particles and magnetic field, which is known as a pulsar wind nebula (PWN), is formed between the termination shock and the supernova shell (for general reviews, see Gaensler & Slane 2006; Kirk, Lyubarsky & Petri 2007; Bucciantini 2008a). This way, the spin-down energy lost by the pulsar through its wind becomes detectable as non-thermal radiation, mostly synchrotron.

The steady progress of X-ray astronomy has resulted in the discovery of a rather peculiar jet–torus structure in the inner part of the Crab Nebula, not predicted by the classical model of plerions. This structure had been seen in earlier observations by Brinkmann, Aschenbach & Langmeier (1985) and Hester et al. (1995), but the recent observations using the *Chandra* X-ray satellite and the *Hubble Space Telescope* show the structure and its temporal nature in spectacular detail (Weisskopf et al. 2000; Hester et al. 2002). Similar structures are found in many other PWNe (Hester et al. 1995; Gotthelf & Wang 2000; Weisskopf et al. 2000; Gaensler, Pivovaroff & Garmire 2001; Helfand, Gotthelf & Halpern 2001; Gaensler et al. 2002; Lu et al. 2002; Pavlov et al. 2003; Romani & Ng 2003; Camilo et al. 2004; Slane et al. 2004).

The first theoretical models for the formation of both the equatorial torus and the polar jets, that combine to form the jet–torus, were presented by Bogovalov & Khangoulian (2002) and Lyubarsky (2002). Both these models agree in that the torus arises due to the anisotropic distribution of the PW power, enhanced in the equatorial direction, and the jets are formed downstream of the wind-termination shock. In particular, Lyubarsky (2002) proposed that jets are produced via the so-called 'tooth-paste' effect related to the hoop stress of the azimuthal magnetic field carried by the wind. These theoretical models were confirmed, including the 'tooth-paste' effect, by series of recent numerical simulations (Komissarov & Lyubarsky 2003, 2004; Del Zanna, Amato & Bucciantini 2004; Bogovalov et al. 2005), performed using newly developed codes for relativistic magnetohydrodynamics (RMHD). The RMHD model of PWNe has been recently developed to a high degree of sophistication and has proven itself capable of explaining, at least qualitatively, many properties of PWNe, including

⋆E-mail: nfcamus@maths.leeds.ac.uk (NFC); serguei@maths.leeds.ac.uk (SSK)

their morphology, polarization, spectral index maps and gamma-ray emission (Bucciantini et al. 2005; Del Zanna, Volpi & Bucciantini 2006; Volpi et al. 2008, 2009).

Although the global structure of Crab's jet–torus appears to be quite persistent over long time-scales, it has been known since 1920s that its fine structure shows a short time variability both in the vicinity of the termination shock and at larger distances (Lampland 1921; Scargle 1969). The most fascinating variable features are the thin synchrotron emitting filaments, dubbed by Scargle (1969) as wisps, who concluded that they may move outwards with relativistic speeds. However, it is the recent high-resolution optical and X-ray monitoring observations of the Crab Nebula that have enabled us to firmly establish that this is indeed the case (Tanvir, Thompson & Tsikarishvili 1997; Hester et al. 2002). They have also discovered the jet variability. In particular, the proper motion of the jet-emission pattern clearly indicates relativistic outflow. Moreover, rather bright and variable features appear near the jet base, like the so-called *sprite* (Hester et al. 2002).

Scargle (1969) commented that the wisps could be either (1) inhomogeneities advected by the flow in the nebula or (2) magnetosonic waves. Later, Gallant & Arons (1994) noted that if ions are part of the PW, then downstream of the termination shock their Larmor radius can be comparable to the separation between the brightest wisps of the Crab Nebula, and thus the wisps may also reflect the steady kinetic structure of the termination shock as mediated by the ions. This idea was recently developed further by Spitkovsky & Arons (2004) who have shown that the cyclotron instability of ions may lead to the excitation of magnetosonic waves in the electron–positron component of the post-termination-shock flow, and thus explain the observed variability of the wisps. Begelman (1999) proposed an alternative, purely magnetohydrodynamic (MHD) model of the wisp origin. He assumed that the flow behind the termination shock consists of a fast equatorial zone and a slower moving surrounding zone, and that the shear between the zones gives rise to the Kelvin–Helmholtz instability which causes the equatorial zone to ripple, these moving ripples are identified with the dynamic wisps of the Crab Nebula. Recently, Bucciantini & Del Zanna (2006) argued that the growth rate of the Kelvin–Helmholtz instability is too slow to explain the wisps in this way. On the other hand, the previous RMHD simulations of PWN did indicate notable variability of the flow and suggested the possibility of explaining the wisp production in the MHD framework (Komissarov & Lyubarsky 2004; Bogovalov et al. 2005; Volpi et al. 2008).

In order to explore whether the observed variability of the Crab Nebula can indeed be explained within the purely MHD approach, we have carried out new RMHD simulations with the highest numerical resolution so far and developed new sophisticated method for the construction of synthetic maps of the synchrotron emission from the simulated PWN. In addition, we did not impose the reflective boundary in the equatorial plane. The simulations have revealed the highly unsteady non-linear behaviour of the termination shock and the highly intricate fibrous structure of the PWN emission, including bright moving wisps. Here, we briefly describe the key results of this study whereas the full account will be given elsewhere.

2 DETAILS OF NUMERICAL SIMULATIONS

To perform these simulations, we used an improved version of the RMHD scheme constructed by Komissarov (1999). In order to reduce numerical diffusion, we apply parabolic reconstruction instead of the linear one of the original code. Our procedure, in brief, is to calculate the minmod-averaged first and second derivatives and to use the first three terms of the Taylor expansion for spatial reconstruction.

2.1 Computational grid and initial solution

We utilize a spherical grid with standard coordinates $\{r, \theta\}$, where in the θ direction we adopt a fixed angular cell size $\Delta\theta$. In the radial direction, we adopt a logarithmic scaling, with radial cell spacing growing as $\Delta r_i = r_i\ \Delta\theta$. As the Courante stability condition requires $\Delta t < \Delta r_i/c$, we split the computational domain into a set of rings such that the outer radius of each ring is twice its inner radius, and advanced the solution in each jth ring with its own time-step Δt_j, where $\Delta t_{j+1} = 2\Delta t_j$. In order to ensure that the termination shock is always fully inside the computational domain and to reduce the computational cost, which is dominated by the inner rings, the number of rings is variable and is kept to the minimum needed to capture the termination shock. If the termination shock moves very close to the inner boundary, an additional inner ring is activated. When it moves outside of the inner ring, this ring is deactivated. Moreover, in order to reduce the computational cost further more, we do not update the cells which are fully inside the PW zone. In order to verify the convergence of numerical solutions, in the statistical sense, we used four grids with 100, 200, 400 and 800 cells in the θ direction. In this paper, we only present the results obtained with the highest resolution, which exceeds by the factor of 4 the resolution of previous simulations.[1] In the radial direction, the computational domain extends up to the distance corresponding to $r = 10$ light-*year* and the simulations are run up to the time corresponding to the current age of the Crab Nebula, $t \approx 960$ yr.

The initial PW zone is spherical with the radius $r_{\rm w} = 0.5$ light-*year*. The wind model is exactly the same as in Komissarov & Lyubarsky (2004) with the magnetization parameter $\xi = 0.4$, the Lorentz factor $W = 10$, and purely azimuthal magnetic field changing sign at $\theta = \pi/2$ according to the model of dissipation of the alternating component of magnetic field of striped wind at the termination shock by Lyubarsky (2003b). Initially, the region outside of the wind zone is filled with cold radially expanding flow with constant density ρ_e and velocity $v \propto r$. The parameters of this flow are selected in such a way that its total mass and kinetic energy within the radius $r_e = 1.47$ light-*year* are $6\,{\rm M}_\odot$ and 10^{51} erg, respectively. This leads to the final size of the simulated PWN that is consistent with the observations. Given the age of the Crab Nebula, it is not expected to have entered the reverberation stage and thus the interaction of the supernova shell with ISM is not important for the dynamics of the PWN. For this reason, we do not introduce the ISM zone and continue the supernova shell solution up to the outer boundary of the computational domain.

At $\theta = 0$ and π, we impose the standard axisymmetric boundary conditions using three ghost cells. At the outer radial boundary, $r = 10$ light-*year*, we imposed the non-reflective boundary conditions and at the inner radial boundary our boundary conditions describe the supersonic PW.

Finally, we adopt the equation of state of ideal gas with the ratio of specific heats $\gamma = 4/3$.

[1] The full account of the convergence study will be given in the follow-up paper.

2.2 Model of synchrotron emission

The synchrotron particles are assumed to be continuously injected at the termination shock with the power-law spectrum

$$f(\epsilon) = A\epsilon^{-\Gamma} \quad \text{for} \quad \epsilon \leqslant \epsilon_{\rm c}, \tag{1}$$

where the cut-off energy is set to the value $\epsilon_{\rm c} = 1000\,\text{TeV}$ and the power index to $\Gamma = 2.2$. According to the results of Kennel & Coroniti (1984b) and Volpi et al. (2008), this simplified model fits the synchrotron spectrum of the Crab Nebula from the optical frequencies to X-rays. In fact, the value of Γ is sensitive to the model of the nebula flow. Moreover, the origin of radio-emitting electrons is unclear and the injection spectrum may have a low-energy cut-off close to the optical energies. Although these details are important for the spectrum studies, they are unlikely to have strong effect on the appearance of the nebula at any given frequency between optics and X-rays. The key factors here are the variation of magnetic field strength and the adiabatic and synchrotron energy losses as they have strong effect on the relative brightness of various features.

In order to account for the adiabatic losses (or gains), a new dynamic variable, the number density of trace species n, is introduced in the simulations; the variation of n reflects the compression, or rarefaction, of the fluid element that carries them around. The covariant equation describing its evolution is

$$\nabla_\mu (n u^\mu) = 0, \tag{2}$$

where u^μ is the four-velocity of the flow. In order to deduce the total expansion experienced by a particular fluid element downstream of the termination shock, we also need to know n_0, the value of n when this element crossed the shock; the volume expansion is then given by the ratio n/n_0. This is achieved via treating n_0 as another dynamic variable which, downstream of the termination shock, satisfies the transport equation

$$\nabla_\mu (n_0 n u^\mu) = 0. \tag{3}$$

Upstream of the shock, we assume that n_0 equals to n and that n is proportional to the total energy flux, i.e.

$$n(r,\theta) = N\left(\frac{r_0}{r}\right)^2\left(\sin^2\theta + \frac{1}{\sigma_0}\right), \tag{4}$$

where r_0, N and σ_0 are constants. For simplicity, we assume that, up to a constant coefficient, the parameter A in equation (1) equals to n_0. The downstream distribution function of the synchrotron electrons can now be expressed as

$$f(\epsilon) = A\left(\frac{n_0}{n}\right)^{-\frac{2+\Gamma}{3}}\left(1-\frac{\epsilon}{\epsilon_\infty}\right)^{\Gamma-2}\epsilon^{-\Gamma}, \quad \epsilon < \epsilon_\infty, \tag{5}$$

where ϵ_∞ is the new cut-off energy due to the synchrotron and adiabatic losses. This is another dynamical variable which is evolved in the simulations according to the transport equation

$$\nabla_\mu (\epsilon_\infty n^{\frac{2}{3}} u^\mu) = -\widetilde{c_2} B^2 \epsilon_\infty^2 n^{\frac{2}{3}}, \tag{6}$$

where B is the magnetic field strength as measured in the fluid frame and $\widetilde{c_2} = (4e^4/9m^4c^7)$. In the derivation, we assumed effective pitch-angle scattering of the electrons (and positrons). Upstream of the termination shock, we set $\epsilon_\infty = \epsilon_{\rm c}$. The corresponding synchrotron emissivity, as measured in the observer's frame, is then calculated using the approximation

$$\mathcal{J}_{\nu_{\rm ob}} \propto n_0 \mathcal{D}^2 B_\perp \left(\frac{n_0}{n}\right)^{-\frac{\Gamma+2}{3}} \epsilon^{1-\Gamma}\left(1-\frac{\epsilon}{\epsilon_\infty}\right)^{\Gamma-2}, \tag{7}$$

where $\nu = c_1 B_\perp \epsilon^2, c_1 = 3e/4\pi m^3 c^5$, $B_\perp$ is the component of the magnetic field normal to the line of sight in the fluid frame and $\mathcal{D} = \nu_{\rm ob}/\nu$ is the Doppler factor.

3 RESULTS AND DISCUSSION

Fig. 1 shows the solution by the end of the simulation run, $t = 954$ yr. Compared to our previous simulations, the most remarkable feature of this solution is the absence of the equatorial disc-like outflow and the large-scale circulation in the nebula. Instead, we observe a rather irregular flow that can be described as a collection of large-scale vortexes. Since the same behaviour is found even in the low-resolution runs, we conclude that the key factor leading to this change in the properties of the PWN flow is the relaxation of the equatorial symmetry condition. These vortexes pick up mass from the interface between the PWN and the supernova shell and transport it into the nebula's interior, creating the intricate fine structure of the density distribution. The long 'fingers' protruding inside the nebula along the polar axis are produced by the backflow of the polar jets contaminated with the entrained mass of the supernova shell. In the proper three-dimensional case, we do not expect the polar jets to remain so straight and collimated as in our simulations. As the result, the backflow will be much less pronounced and coherent.

Fig. 2 illustrates the highly complex dynamics found in the central part of the simulated PWN. The structure of the termination shock is highly variable due to the non-linear interactions with the flow inside the nebula. On the one hand, both the size and the shape of the shock change constantly due to 'collisions' with the large amplitude waves and vortexes of the nebula. On the other hand, these changes in the shock structure result in highly variable outflow from the shock. Thus, the variations of the termination shock structure and the variability of the flow in the nebula feed on each other, and at this stage it is quite impossible to distinguish between the cause and the effect (this is analogous to the famous 'hen and egg' problem). This behaviour of the PW termination shock is reminiscent of that of the accretion shock in problems involving supersonic accretion (e.g. Blondin, Mezzacappa & DeMarino 2003; Buras et al. 2006; Scheck et al. 2008) and suggests the possibility of common origin. The characteristic time-scale of the large-scale variations is around 1 to 2 years. This makes sense as the length-scale of the termination shock is about 1 light-year and the speed of magnetosonic waves is close to the speed of light.

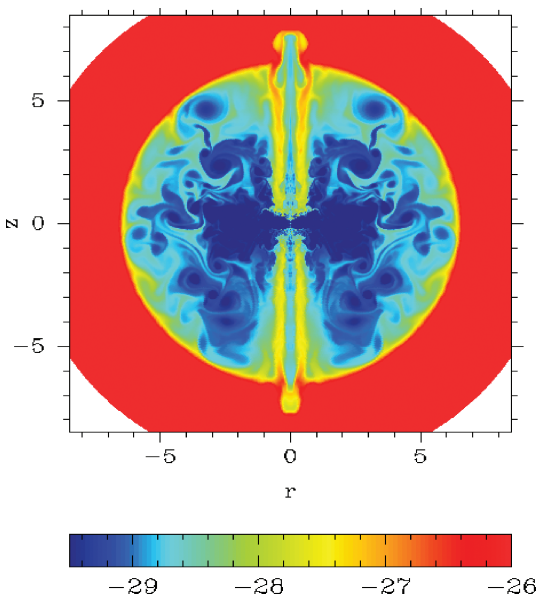

Figure 1. The plot shows $\log_{10}\rho$ in dimensionless units. The unit of length in this and other plots is 1 light-year.

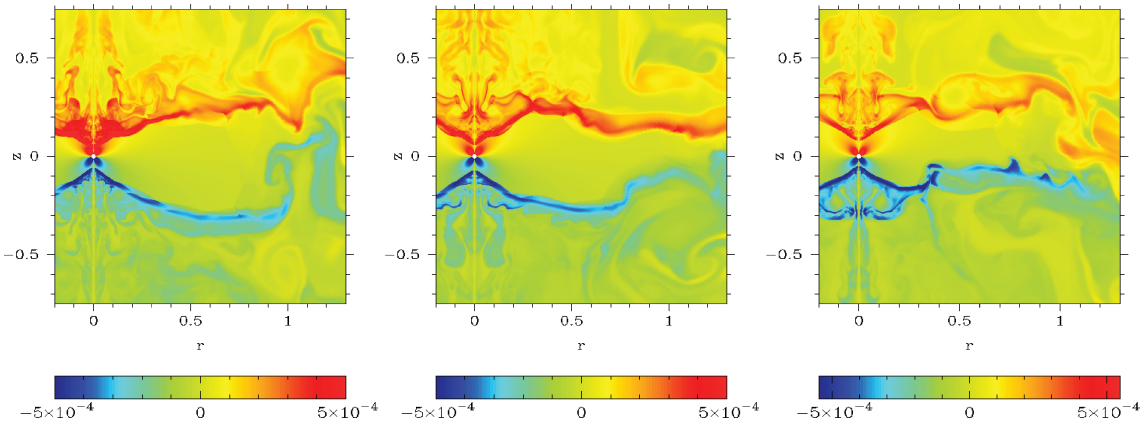

Figure 2. All plots show the azimuthal component of magnetic field in CGS units and clearly illustrate the non-linear dynamics of the termination shock. The left-hand panel shows a stage at which the termination shock is fully inflated ($t = 912.3$ yr). The middle panel shows the northern shock structure being distorted ($t = 926.6$ yr). The right-hand panel shows the shock complex to be highly compressed ($t = 933.1$ yr).

In contrast to the PW, the equatorial symmetry in the PWN is completely broken and often the fluid elements blown by the wind into the Southern hemisphere (in Fig. 2 they are coloured in blue) end up in the Northern hemisphere, and the other way around. Similarly strong breakdowns of equatorial symmetry have been observed in the simulations of stellar collapse (e.g. Scheck et al. 2008; Komissarov 2009). This seems to be a general rule for the problems where the shocked plasma is confined to a finite or slowly expanding volume.

As expected, and in agreement with previous simulations, the predominant motion near the equatorial plane is an outflow. The typical speed of this outflow inside the inner 2 light-year is around $0.6c$. The outflow is highly inhomogeneous with regions of strong magnetic field following regions of relatively weak field. Such strong variations in magnetic field strength lead to strong variations of synchrotron emissivity and ultimately to the phenomenon of expanding wisps (see Fig. 3). Further out, but well before reaching the supernova shell, the outflow slows down and mixes with the rest of the PWN.

Above the equatorial plane, a backflow with superimposed vortexes can also be seen. This seems to be the reason for the contracting wisps occasionally observed in these simulations. Closer to the symmetry axis, with $r < 0.5$ light-year, another backflow is seen. Like in the previous simulations, this flow originates from the highly magnetized layers of recently shocked plasma of the PW. The strong magnetic hoop stress in these layers stops the outflow and turns it back towards the axis. The resultant axial compression drives the polar jets in a fashion reminiscent of the tooth-paste flow. The axial pinch is rather non-uniform and the flow structure at the jet base is highly variable. One can interpret this variability as the development of the 'sausage' instability enhanced by the fact that the backflow is already highly inhomogeneous and the instability is in the non-linear regime from the start. The converging magnetosonic compression waves, which originate in the dynamically

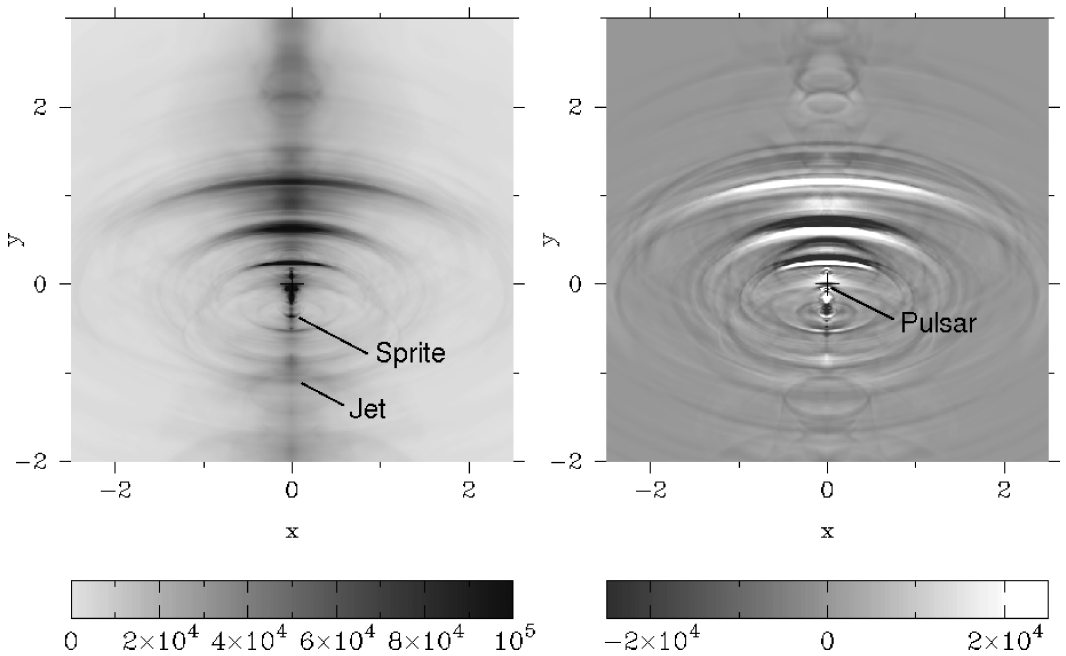

Figure 3. The left-hand panel shows the synthetic optical synchrotron image of the simulated PWN at time 911.0 years (linear scale). The right-hand panel shows the difference between two optical images obtained at the same epoch and separated by approximately 105 days.

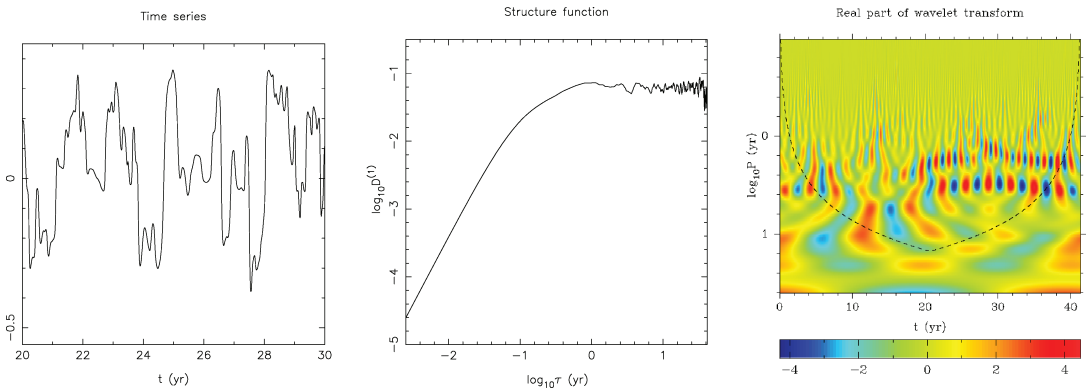

Figure 4. The left-hand panel shows the fragment of time-series data for the comoving magnetic field (in arbitrary units) at the reference cell with coordinates $r = 1.75$ light - *year*, $\theta = 87^\circ$. Time is measured from the start of sampling. The middle panel shows the structure function of this time-series. The right-hand panel shows the real part of its wavelet transform using the Morlet mother wavelet; the dashed line corresponds to the cone of influence.

active region around the equatorial outflow, also contribute to this process. In the synthetic synchrotron maps, this region often shows relatively compact and bright variable features (see Fig. 3) which look similar to the Crab's 'sprite' (Hester et al. 2002).

The variability of the Crab Nebula emission was investigated by Hester et al. (2002) via subtraction of two images separated by approximately 109 days. In particular, an outward moving wisp appears on the resultant image as a dark wisp followed by a bright one. In Fig. 3, we apply the same technique to our synthetic optical images. The dynamics of simulated wisps are remarkably similar to that of the real ones. In agreement with the observations, the typical apparent speed of the wisps is $\simeq$0.5c within the inner $\simeq$2 light-year (in the mapping procedure, we ignore the time-delay effect.). Further out, the apparent speed of the wisps significantly decreases, and we often observe wisp mergers like those described in Hester et al. (2002). Such behaviour agrees with the interpretation of wisps as magnetic inhomogeneities advected by a non-uniform decelerating subsonic flow.

Having observed the wisp production in our RMHD simulations, we then quantitatively analysed the nature of the nebula variability in order to establish whether the shock dynamics and associated synchrotron emission show any periodicity, and if not, to determine the statistical nature of the fluctuations. A number of time-series were constructed by measuring fluid parameters at the point with coordinates $(r, \theta) = (1.75\,\text{light-}year, 87^\circ)$ after each local time-step. The left-hand panel of Fig. 4 shows part of such time-series for the comoving magnetic field. The middle panel of Fig. 4 shows the structure function of the time-series. One can see that it has a plateau at long time lags and a broken power law at short time lags. The hard power law at time lags $\tau < 0.08$ yr is clearly a numerical noise as this time-scale corresponds to the numerical resolution of our simulations. The softer power law at time lags $\tau = 0.1$–1 yr corresponds to well-resolved scales and presumably captures the MHD turbulence developed in the simulations. The transition to plateau at $\tau \simeq 1.0$ yr indicates the characteristic time-scale for the large-scale process that drives the turbulence. The only candidate for such a process is the oscillation of the termination shock. This oscillation cannot occur on scale below the light-crossing time of the shock, and this seems to explain the characteristic time-scale revealed by the structure function.

In order to investigate this issue further, we also applied the method of wavelet transform. In the right-hand panel of Fig. 4, the real part of the wavelet transform for the Morlet mother wavelet (Torrence & Compo 1998) is shown. One can see clear evidence of quasi-periodic oscillations with the quasi-period $P = 1.5$–3 yr. The analysis of time-series for other flow parameters gives similar results.

The available variability data for the Crab Nebula do not cover sufficiently long time-period and are too scarce for rigorous statistical analysis. Therefore, we cannot yet make proper comparison between the observations and our simulations. The observations by Hester et al. (2002) revealed two wisps produced within 1 year. This may indicate a somewhat shorter characteristic time-scale for wisp production compared to other results, but may also be just a local variation. Under the circumstances, we conclude that the MHD model explains not only the structure of the Crab Nebula but also its variability reasonably well.

ACKNOWLEDGMENTS

NFC was supported by the UK Science and Technology Facilities Council (STFC). SSK was supported by STFC through the rolling grant 'Theoretical astrophysics in Leeds'. NB was supported by NASA through Hubble Fellowship grant HST-HF-01193.01-A, awarded by the Space Telescope Science Institute, which is operated by the Association of Universities for Research in Astronomy, Inc., for NASA, under contract NAS 5-26555.

REFERENCES

Begelman M. C., 1999, ApJ, 512, 755
Blondin J. M., Mezzacappa A., DeMarino C., 2003, ApJ, 584, 971
Bogovalov S. V., Khangoulian D. V., 2002, MNRAS, 336, L53
Bogovalov S. V., Chechetkin V. M., Koldoba A. V., Ustyugova G. V., 2005, MNRAS, 358, 705
Brinkmann W., Aschenbach B., Langmeier A., 1985, Nat, 313, 662
Bucciantini N., 2008, Advances Space Res., 41, 491
Bucciantini N., Del Zanna L., 2006, A&A, 454, 393
Bucciantini N., Del Zanna L., Amato E., Volpi D., 2005, A&A, 443, 519
Buras R., Janka H.-Th., Rampp M., Kifonidis K., 2006, A&A 457, 281
Camilo F., Gaensler B. M., Gotthelf E. V., Halpern J. P., Manchester R. N., 2004, ApJ, 616, 1118
Del Zanna L., Amato E., Bucciantini N., 2004, A&A, 421, 1063
Del Zanna L., Volpi D., Bucciantini N., 2006, A&A, 453, 621
Gallant Y. A., Arons J., 1994, ApJ, 435, 230
Gaensler B. M., Slane P. O., 2006, Ann. Rev. Astron. Astrophys., 44, 17
Gaensler B. M., Pivovaroff M. J., Garmire G. P., 2001, ApJ, 556, L107
Gaensler B. M., Arons J., Kaspi V. M., Pivovaroff M. J., Kawai N., Tamura K., 2002, ApJ, 569, 878

Gotthelf E. V., Wang Q. D., 2000, ApJ, 532, L117
Helfand D. J., Gotthelf E. V., Halpern J. P., 2001, ApJ, 556, 380
Hester J. J. et al., 1995, ApJ, 448, 240
Hester J. J. et al., 2002, ApJ, 577, L49
Kennel C. F., Coroniti F. V., 1984a, ApJ, 283, 694
Kennel C. F., Coroniti F. V., 1984b, ApJ, 283, 710
Kirk J. G., Lyubarsky Y., Petri J., 2007, preprint (astro-ph/0703116)
Komissarov S. S., 1999, MNRAS, 303, 343
Komissarov S. S., Barkov M. V., 2009, MNRAS, 397, 1153
Komissarov S. S., Lyubarsky Y. E., 2003, MNRAS, 344, L93
Komissarov S. S., Lyubarsky Y. E., 2004, MNRAS, 349, 779
Lampland C. O., 1921, PASP, 33, 79
Lu F. J., Wang Q. D., Aschenbach B., Durouchoux P., Song L. M., 2002, ApJ, 568, L49
Lyubarsky Y. E., 2002, MNRAS, 329, L34
Lyubarsky Y. E., 2003b, MNRAS, 345, 153
Pavlov G. G., Teter M. A., Kargaltsev O., Sanwal D., 2003, ApJ, 591, 1157
Rees M. J., Gunn J. E., 1974, MNRAS 167, 1
Romani R. W., Ng C.-Y., 2003, ApJ, 585, L41
Scargle J. D., 1969, ApJ, 156, 401
Scheck L., Janka H.-Th., Foglizzio T., Kifonidis K., 2008, A&A, 477, 931
Slane P., Helfand D. J., van der Swaluw E., Murray S. S., 2004, ApJ, 616, 403
Spitkovsky A., Arons J., 2004, ApJ, 603, 669
Tanvir N. R., Thompson R. C., Tsikarishvili E. G., 1997, New Astron., 1, 311
Torrence C., Compo G., 1998, Bull. Am. Meteorol. Soc., 79, 61
Volpi D., Del Zanna L., Amato E., Bucciantini N., 2008, A&A, 485, 337
Volpi D., Del Zanna L., Amato E., Bucciantini N., 2009, preprint (arXiv:0903.4120)
Weisskopf M. C. et al., 2000, ApJ, 536, L81

This paper has been typeset from a TEX/LATEX file prepared by the author.